P-Matrix Analysis of Surface Acoustic Waves in Piezoelectric Phononic Crystals

Yahui Tian, Honglang Li, Yabing Ke, Ce Yuan, and Shitang He

Abstract—Large time/memory costs have constituted a significant obstacle for accurately analyzing surface acoustic waves (SAWs) in large-sized two-dimensional (2-D) piezoelectric phononic crystals (PnCs). To overcome this obstacle, this study introduces the unit P-matrix and its associated cascading. To obtain an accurate unit P-matrix, the Y parameters of the SAW delay lines were derived using a three-dimensional (3-D) finite-element model (FEM) with and without 2-D piezoelectric PnCs, respectively, on the transmitting path. A time window function was adopted to extract the desired signals from the P-matrix analysis. Then, unit P-matrix cascading was used to obtain SAW propagation parameters for the large-sized piezoelectric PnCs. Using this method, the SAW in aluminum (Al) /128°-YXLiNbO$_3$ PnCs was analyzed over 150 periods. Experiments were also conducted. To choose the appropriate size of the unit P-matrix, the variance between experimental results and theoretical results, and time/memory cost were compared for different periods. The results indicate that cascading by unit P-matrix of 25 PnCs periods can be appropriately adopted to accurately derive the SAW propagation parameters over 150 periods. This indicates the accuracy of the unit P-matrix derived by 3-D FEM and the effectiveness of P-matrix analysis.

Index Terms—Piezoelectric phononic crystals (PnCs), P-matrix, surface acoustic wave (SAW), three-dimensional (3-D) finite-element method (FEM).

I. Introduction

PIEZOELECTRIC phononic crystals [1] (PnCs) are periodic elastic structures consisting of two different elastic materials, which have the property of band gaps. This property has led to explorations regarding the use of piezoelectric PnCs in bulk acoustic wave (BAW) devices [2]–[7]. Compared with BAW devices, surface acoustic wave (SAW) devices can be used for a greater variety of tasks. Thus, significant research efforts have recently focused on the applications of piezoelectric PnCs in SAW [8]–[12] devices, including weighted SAW waveguides [10] based on piezoelectric PnCs by Tian *et al.*, a SAW resonator with piezoelectric PnCs reported by Solal *et al.* [11], and SAW sensor exploration using photonics, phononics, and microfluidics based on monolithic PnCs [12]. These studies

demonstrate the potential for using piezoelectric PnCs in SAW devices.

Finite-difference time domain (FDTD) [13]–[15], plane wave expansion (PWE) [16]–[18], finite-element method (FEM) [19]–[23], and finite-element method/boundary element method (FEM/BEM) [24] have been developed to analyze SAW propagation in piezoelectric PnCs. Zhao [13] successfully used the FDTD to analyze SAW propagation in piezoelectric PnCs, finding that although the FDTD was simple and efficient, it was inaccurate due to numerical dispersion. PWE was used by Laude [16] and Wu [17], [18] to analyze the band gaps in piezoelectric PnCs, but it provided a suboptimal convergence rate and poor accuracy. Compared to FDTD and PWE, FEM provides high accuracy and has been widely adopted to analyze the SAWs in piezoelectric PnCs. But it requires a long run time and significant memory use. Ventura [24] has combined the FEM with BEM for one-dimensional (1-D) PnCs to reduce time and memory cost. However, this obstacle still exists in two-dimensional (2-D) piezoelectric PnCs, particularly when analyzing SAW propagation parameters in large 2-D piezoelectric PnCs. To overcome this obstacle, this study introduces the P-matrix to 2-D piezoelectric PnCs. The P-matrix [25] has been widely used in SAW devices for many years. Using the cascading P-matrix, the propagation parameters, such as the SAW transmission and reflection coefficients in large piezoelectric PnCs, can be accurately obtained without significant time or memory costs. First, an accurate three-dimensional (3-D) FEM was used to simulate the small-sized piezoelectric PnCs and obtain the unit P-matrix, which requires substantial time and memory. Then, the unit P-matrix was cascaded to obtain the P-matrix of the large-sized piezoelectric PnCs, which requires minimal time and memory via data processing with MATLAB.

In the following discussion, Section II introduces this method in detail, including the P-matrix analysis based on the 3-D FEM and cascading unit P-matrix. Section III uses 2-D aluminum (Al) /128°-YXLiNbO$_3$ PnCs as an example for analyzing the SAW propagation in the large-sized piezoelectric PnCs based on this method. Experiments were also conducted and compared with theoretical results based on different PnC periods in the unit P-matrix. Section IV presents the conclusion.

II. P-Matrix Analysis of SAW in 2-D PnCs Based on 3-D FEM

In this method, two SAW delay lines were adopted as shown in Fig. 1. They consisted of an emitting interdigital transducer (IDT), a receiving IDT, and the transmitting path with or without piezoelectric PnCs, respectively. In this section, the

(a)

(b)
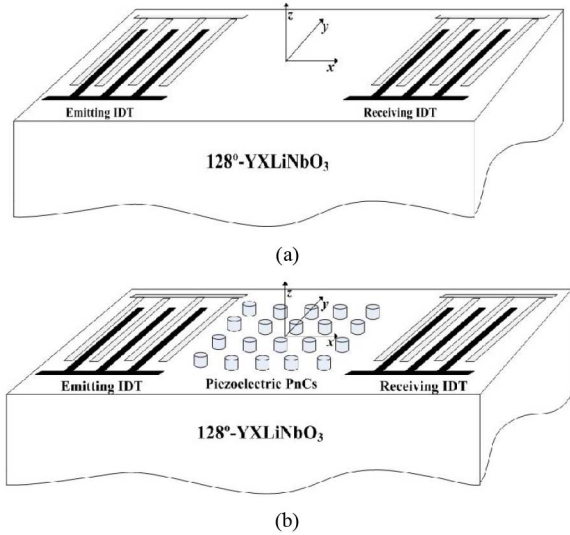
Fig. 1. Two SAW delay lines. (a) Without piezoelectric PnCs on the transmitting path. (b) With piezoelectric PnCs on the transmitting path.
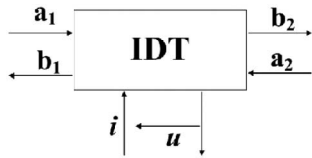
Fig. 2. P-matrix model of an IDT.

P-matrix analysis of the SAW delay lines is primarily described, indicating that the unit P-matrix of the SAW propagation in 2-D piezoelectric PnCs can be derived based on these Y parameters. Next, the 3-D FEM is introduced to calculate these Y parameters. Finally, the cascading of the unit P-matrix is used to obtain the SAW propagation parameters for the large-sized 2-D piezoelectric PnCs.

A. Unit P-Matrix Analysis of SAW in 2-D Piezoelectric PnCs

According to the theory of the P-matrix [25], IDT can be described as a three-port network with two acoustical ports and one electrical port, as shown in Fig. 2 and (1)

$$
\begin{bmatrix} b_1 \\ b_2 \\ i \end{bmatrix} = \begin{bmatrix} P_{11}^{\mathrm{IDT}} & P_{12}^{\mathrm{IDT}} & P_{13}^{\mathrm{IDT}} \\ P_{21}^{\mathrm{IDT}} & P_{22}^{\mathrm{IDT}} & P_{23}^{\mathrm{IDT}} \\ P_{31}^{\mathrm{IDT}} & P_{32}^{\mathrm{IDT}} & P_{33}^{\mathrm{IDT}} \end{bmatrix} \begin{bmatrix} a_1 \\ a_2 \\ u \end{bmatrix} \tag{1}
$$

where a_i is the input of the acoustical ports, b_i is the output of the acoustical ports, u is the voltage of the electrical port, i is the electrical current of the electrical port, and P_{ij}^{IDT} is the P-matrix element of the IDTs.

Differing from IDT, the P matrices of free surface and piezoelectric PnCs transmitting paths can be reduced to two acoustical ports as

$$
\begin{bmatrix} b_1 \\ b_2 \end{bmatrix} = \begin{bmatrix} P_{11} & P_{12} \\ P_{21} & P_{22} \end{bmatrix} \begin{bmatrix} a_1 \\ a_2 \end{bmatrix}. \tag{2}
$$

Based on the P matrices of IDT and transmitting paths, the equivalent models of the two SAW delay lines from Fig. 1 can
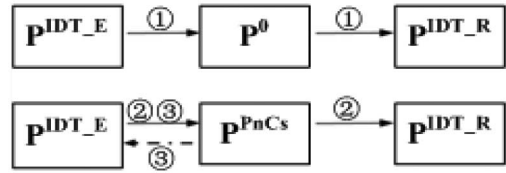
Fig. 3. P-matrix equivalent models of structures in Fig. 1.

be derived as shown in Fig. 3. We assume that the arrangement in Fig. 1 is perfectly symmetric and the emitting IDT and the receiving IDT are the same. Thus, the P matrices of these IDTs are the same.

In Fig. 3, transmitting path ① indicates that the signal transmits from the emitting IDT to the receiving IDT across the free surface. This can be expressed by

$$
Y_{21}^0 = P_{23}^{\mathrm{IDT}} P_{21}^0 \cdot P_{31}^{\mathrm{IDT}} \tag{3}
$$

where Y_{21}^0 is the first signal in the transfer admittance of the SAW delay line with the free-surface transmitting path and P_{21}^0 is the transmission coefficient of the free-surface transmitting path, which can be described by

$$
P_{21}^0 = e^{-j\omega s_f l} \tag{4}
$$

where s_f is the slowness of the free surface and l is the length of the transmitting path.

In transmitting path ②, the signal transmits from the emitting IDT to the receiving IDT across the 2-D piezoelectric PnCs, yielding

$$
Y_{21}^{\mathrm{PnCs}} = P_{23}^{\mathrm{IDT}} P_{21}^{\mathrm{PnCs}} \cdot P_{31}^{\mathrm{IDT}} \tag{5}
$$

where Y_{21}^{PnCs} is the first signal in the transfer admittance of the SAW delay line with the piezoelectric PnCs and P_{21}^{PnCs} is the transmission coefficient of the piezoelectric PnCs.

In transmitting path ③, the signal is sent from the emitting IDT, reflected by the piezoelectric PnCs, and received by the emitting IDT. Thus, the P-matrix provides the relationship as follows:

$$
Y_{11}^{\mathrm{PnCs}\_r} = P_{23}^{\mathrm{IDT}} P_{11}^{\mathrm{PnCs}} \cdot P_{32}^{\mathrm{IDT}} \tag{6}
$$

where $Y_{11}^{\mathrm{PnCs}\_r}$ is the reflected signal of PnCs in the input admittance of the SAW delay line with the piezoelectric PnCs and P_{11}^{PnCs} is the reflection of the piezoelectric PnCs.

By comparing transmitting paths ① and ② with (3) and (5), the transmission coefficient of the piezoelectric PnCs P_{21}^{PnCs} can be obtained via (7) when Y_{21}^0 is not equal to zero

$$
P_{21}^{\mathrm{PnCs}} = \frac{Y_{21}^{\mathrm{PnCs}}}{Y_{21}^0} P_{21}^0. \tag{7}
$$

By comparing transmitting paths ① and ③ with (3) and (6), as P_{32}^{IDT} is equal to P_{13}^{IDT} according to the symmetry of the IDTs, the reflection of the piezoelectric PnCs P_{11}^{PnCs} can be obtained by (8) when Y_{21}^0 is not equal to zero

$$
P_{11}^{\mathrm{PnCs}} = \frac{Y_{11}^{\mathrm{PnCs}\_r}}{Y_{21}^0} P_{21}^0. \tag{8}
$$
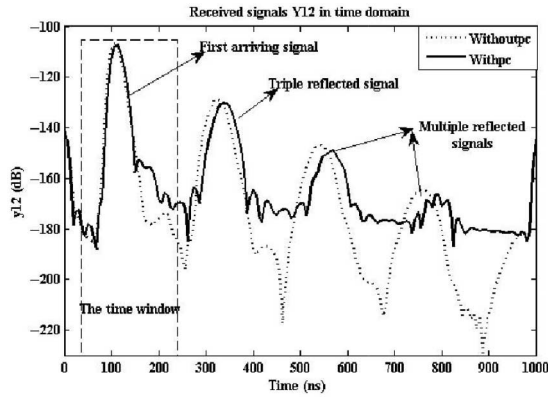
Fig. 4. Signals Y_{12} received in the time domain of the theoretical model.
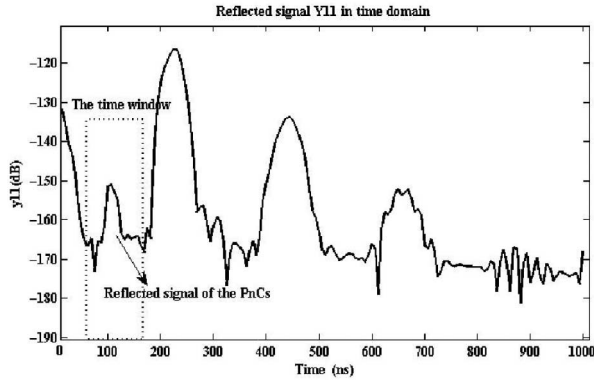
Fig. 5. Signal Y_{11} received in the time domain.

According to the analysis above, Y_{21}^0, Y_{21}^{PnCs}, and $Y_{11}^{\text{PnCs\_}r}$ are needed to calculate the transmission and reflection coefficients.

In the theoretical FEM simulation models, the conventional receiving signals Y_{21} that reach the emitting port include the first-arriving signal, the triple reflected signal, and the multiple reflected signals. We used an inverse Fourier transformation (iFFT) to obtain the first signals of Y_{21}^0 and Y_{21}^{PnCs} from Y_{21} in the two SAW delay lines. Then, the desired signals of the first-arriving signal are derived by adding the time window, shown as a rectangle block in Fig. 4. Finally, we conducted a Fourier transformation (FFT) on the extracted signals.

In Fig. 5, $P_{11}^{\text{PnCs\_}r}$ can be obtained by first subtracting Y_{11} from the two SAW delay lines to remove the direct IDT electrical signal. Then, an iFFT was conducted on the subtracted signal and the time window function was added to extract the first-reflected signal, as shown in Fig. 5. Finally, the FFT of the extracted signal was used to obtain the signal in the frequency domain.

After producing these signals, the transmission and reflection coefficients of the unit cell can be obtained by (7) and (8).

B. Analysis of the 3-D FEM Model

An accurate 3-D FEM model was built to obtain the desired Y parameters, as shown in Fig. 6. In the FEM model, it is assumed that the aperture of the IDT is infinite and the piezoelectric PnCs periods are infinite in this direction. The SAW delay lines
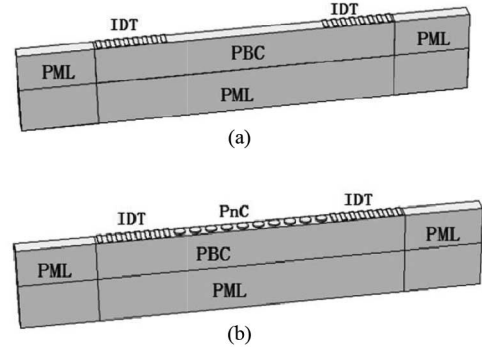
Fig. 6. Three-dimensional FEM of the SAW delay lines. (a) Without piezoelectric PnCs on the transmitting path. (b) With piezoelectric PnCs on the transmitting path.

were reduced to one period by using the period boundary condition (PBC) in this direction. This was undertaken to reduce the model's time and memory costs. On two edges and the bottom of the substrate, a perfect matching layer (PML) was adopted to absorb the wave reflected by the boundary.

In the piezoelectric substrate, the piezoelectric coupling-wave equations are

$$\begin{cases} \rho \frac{\partial^2 u_i}{\partial t^2} - c_{ijkl} \frac{\partial^2 u_k}{\partial x_j \partial x_l} - e_{ijk} \frac{\partial^2 \varphi}{\partial x_j \partial x_k} = 0 \\ e_{jkl} \frac{\partial^2 u_k}{\partial x_j \partial x_l} - \varepsilon_{jk} \frac{\partial^2 \varphi}{\partial x_j \partial x_k} = 0 \end{cases} \tag{9}$$

where $i, j, k, l = 1, 2, 3$, u_i is the displacement element, φ is the electric potential, ρ is the mass density of the material, ε is the permittivity, e is the piezoelectric constant, and c is elastic stiffness constant.

The PBC satisfies the Bloch periodic theorem, which indicates that the structure exhibits translational periodicity. Thus, the physical fields of the two sides are equal in the amplitude for one period, as follows:

$$\Phi|_{y=0} = \Phi|_{y=b} \tag{10}$$

where ϕ represents the physical fields, including the displacement U, the stress T, and the strain S, and b denotes the lattice constant of 2-D piezoelectric PnCs.

A lossy medium was introduced in the PML areas, in which the waves decay rapidly. The attenuation factor of the medium is usually expressed by [26]

$$\sigma(x) = \sigma_{\max}(x/d)^2 \tag{11}$$

where x denotes the distance from the inner boundary of the PML area, d is the thickness of the PML layers, and $\sigma_{\max}$ is the maximum attenuation on the PML outer boundary.

On the upper surface of the piezoelectric substrate, the free-surface boundary conditions are satisfied by

$$\text{T}_{3i}|_{z=0} = 0, \quad (i = 1, 2, 3). \tag{12}$$

Displacement and stress in the area of the IDT and the 2-D piezoelectric PnCs are continuous, satisfied by

$$\begin{cases} T_{3i}|_{z=0^+} = T_{3i}|_{z=0^-} \\ u_i|_{z=0^+} = u_i|_{z=0^-} \end{cases} \quad (i = 1, 2, 3). \tag{13}$$

Equation (14) describes the IDT in the electric domain analysis

$$\begin{bmatrix} i_1 \\ i_2 \end{bmatrix} = \begin{bmatrix} Y_{11} & Y_{12} \\ Y_{21} & Y_{22} \end{bmatrix} \begin{bmatrix} u_1 \\ u_2 \end{bmatrix} \tag{14}$$

where i_1 and i_2 represent the current in the emitting IDT and receiving IDT, respectively, u_1 and u_2 represent the voltage in the emitting IDT and receiving IDT, respectively, and Y is the admittance of the SAW delay line.

In the FEM model, we imposed 1 V on the emitting IDT and grounded the receiving IDT. Thus, according to (14), we obtained Y_{11} and Y_{21} via

$$\begin{cases} Y_{11} = i_1 \\ Y_{21} = i_2. \end{cases} \tag{15}$$

Therefore, we can obtain Y_{11} and Y_{21} via the charge distribution Q, derived by the FEM simulation according to

$$i = jwQ. \tag{16}$$

The models were built and analyzed using FEM software. First, the geometric structures of the models were established. Then, the material constants were added to the structures. Next, the boundary conditions and initial field conditions were set. The boundary conditions included the PBC, PML, free-surface, and electrical boundary conditions (the IDTs had one potential terminal and one ground terminal, and the metal pillars were set as equipotential bodies with zero-surface charge). The initial field condition was set to 1 V potential at the potential terminal in the emitting IDT to generate the acoustic filed. We then meshed generations at no less than ten meshes every wave length to guarantee the accuracy of the calculation. The wave length we adopted here is equal to the period of the pillars. We selected the frequency domain in the software, meaning that simulations were conducted in the frequency domain, and we could adjust the frequency range as needed. Finally, calculations can begin and all of the physical field distributions can be obtained, including the charge field. Thus, we can derive the Y parameters from the charge analysis.

C. Unit P-Matrix Cascading

The unit P-matrix of the small-sized piezoelectric PnCs can be obtained from the previous analysis. To obtain the propagation parameters of the SAWs in the large-sized piezoelectric PnCs, the unit P-matrix cascading was introduced.

To be able to ensure the cascading correctly, the input and output phase planes of the wave amplitudes in the unit have been set away from the center of the first column and the last column of the pillars in the unit.

As shown in Fig. 7, assuming that the PnCs are infinite in the direction perpendicular to the direction of wave propagation, the P-matrix of a larger unit can be obtained by unit P-matrix cascading. The combined P-matrix is described as follows:

$$\begin{cases} P_{11} = P_{11}^A + P_{11}^B \dfrac{P_{21}^A P_{12}^A}{1 - P_{11}^B P_{22}^A} \\ P_{12} = P_{21} = \dfrac{P_{12}^A P_{12}^B}{1 - P_{11}^B P_{22}^A} \\ P_{22} = P_{22}^B + P_{22}^A \dfrac{P_{21}^B P_{12}^B}{1 - P_{11}^B P_{22}^A}. \end{cases} \tag{17}$$
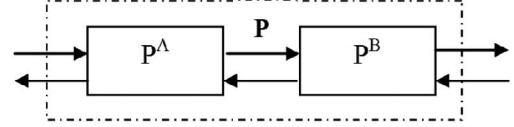
Fig. 7. P-matrix cascading.

Based on the theory above, the P-matrix of the large-sized piezoelectric PnCs can be derived with the unit P-matrix via cascading.

III. ANALYSIS OF THE SAWs IN THE 2-D AL/128°-YXLINBO₃ PNCS AND ADDITIONAL EXPERIMENTS

A. P-Matrix Analysis of the SAW in the 2-D Piezoelectric Al/128°-YXLiNbO₃ PnCs

As an example, the transmission coefficient and reflection of the SAW were analyzed in 150 periods of piezoelectric Al/128°-YXLiNbO₃ PnCs.

The structural parameters of the models are as follows: the lattice constant, the thickness, and the diameter of aluminum stubs are 12, 0.6, and 7 μm, respectively. Only four pairs of electrodes in both the emitting IDT and the receiving IDT were applied to obtain the wideband range of working frequency. Considering the Bragg reflection, the period of the electrodes is 12 μm, which is equal to the lattice constant, and the metallization ratio is 0.5. Because the center frequency of the SAW delay lines is approximately 320 MHz and the bandwidth is approximately 80 MHz, we set the calculation frequency range from 240 to 400 MHz, which encompasses the main portion of the SAW delay lines' responses. The material parameters of the aluminum are as follows: the density is 2730 kg/m³, the Young modulus is 7.76×10^{10} Pa, and the Poisson ratio is 0.352. The material parameters of 128°-YXLiNbO₃ are as follows: the density is 4700 kg/m³, and the stiffness constant, piezoelectric strain constants, and relative dielectric constants are [27]

$$[c] = \begin{bmatrix} 2.03 & 0.7007 & 0.5793 & 0.1285 & 0 & 0 \\ 0.7007 & 1.9442 & 0.9076 & 0.0967 & 0 & 0 \\ 0.5793 & 0.9076 & 2.2205 & 0.0853 & 0 & 0 \\ 0.1285 & 0.0967 & 0.0853 & 0.7576 & 0 & 0 \\ 0 & 0 & 0 & 0 & 0.5695 & -0.0510 \\ 0 & 0 & 0 & 0 & -0.0510 & 0.7805 \end{bmatrix}$$

$$\times 10^{11}$$

Pa $[d] =$

$$\begin{bmatrix} 0 & 0 & 0 & 0 & 0.7944 & 0.0877 \\ -0.1716 & 0.6329 & -0.4366 & 0.0703 & 0 & 0 \\ 0.1214 & -0.4735 & 0.3836 & -0.0118 & 0 & 0 \end{bmatrix}$$

$$\times 10^{-10} C/N$$

$$[\varepsilon]^S = \begin{bmatrix} 44 & 0 & 0 \\ 0 & 38.3144 & -7.2772 \\ 0 & -7.2772 & 34.6856 \end{bmatrix}.$$
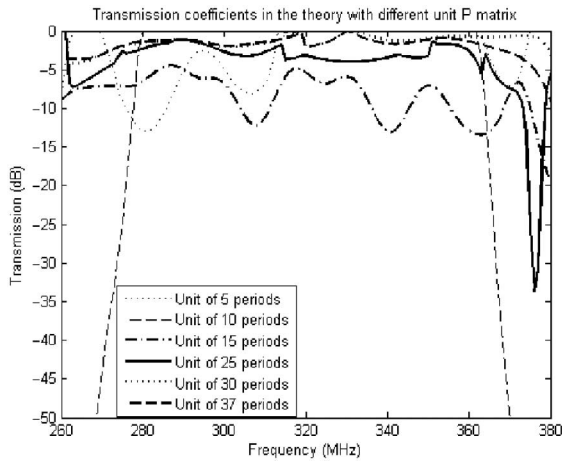
Fig. 8. Transmission coefficients for different unit P matrices.

Fig. 9. Measured Y_{12} of SAW delay lines, respectively, with and without PnCs.

Fig. 10. RMS error and memory cost of different periods in the unit.

TABLE I
TIME COST WITH DIFFERENT PnCs PERIODS IN THE UNIT

Periods in the unit	5	10	15	25	30	37
Time cost (min)	229	369	512	664	724	938

Based on the structural and material parameters above, different unit models with Al/128°-YXLiNbO$_3$ PnCs periods of 5, 10, 15, 25, 30, and 37 were analyzed to compare different results based on different unit P matrices. Then, the SAW propagation transmission coefficients of the 150 periods of the piezoelectric Al/128°-YXLiNbO$_3$ PnCs were derived based on different unit P-matrix cascading results, as shown in Fig. 8. Because the transmission coefficients in the 240 to 260 MHz and 380 to 400 MHz ranges are much smaller than the 260 to 380 MHz value, we have limited the frequency range from 260 to 380 MHz to choose the appropriate Y scale. Fig. 8 shows that the transmission coefficient curves tend to converge for unit P-matrix with periods of 25, 30, and 37 for the Al/128°-YXLiNbO$_3$ PnCs. They exhibit a large divergence and ripples for the unit P-matrix of 5, 10, and 15 periods. This may be due to the problem that for short crystals, the successive reflected signals are not well separated in the time domain and are not separated correctly when performing the gating.

B. 2-D Piezoelectric Al/128°-YXLiNbO$_3$ PnCs Experiments

To verify the theoretical results, further experiments were also conducted. First, two SAW delay lines consisting of four pairs of electrodes in the emitting IDT and the receiving IDT, and with or without 150 periods of 2-D Al/128°-YX-LiNbO$_3$ PnCs, were fabricated using microelectromechanical-system (MEMS) technology. The structural parameters adopted in the experiments are the same as in the theory.

Then, the Y parameters of the SAW delay lines were measured using the network analyzer, with and without piezoelectric PnCs. The measured Y_{12} parameters in the experiments are displayed in Fig. 9. From Fig. 9, it can be seen the main lobe occurred from 260 to 340 MHz and fluctuations existed in the responses.

To remove the meaningless signals, including the triple reflected signal, the rectangular time window was introduced to extract the desired signals in the time domain. Thus, the transmission coefficient and reflection of the SAW propagation in the 2-D piezoelectric PnCs were obtained via (7) and (8).
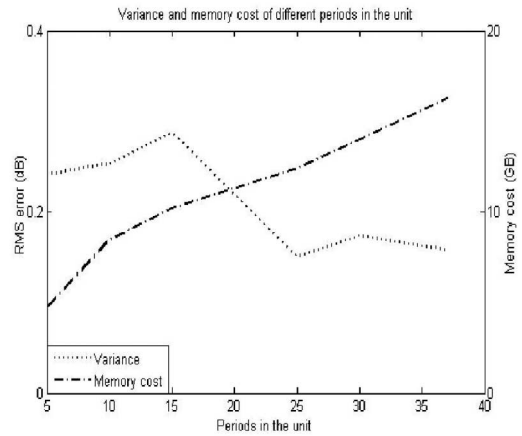
C. Comparison of the Results of the P-Matrix Analysis and the Experiments

The theoretical and experimental results were compared, and the time and memory costs were analyzed to choose the appropriate unit P-matrix size.

The root-mean-square (RMS) error of transmission coefficient between the experiments and theory was calculated by

$$R = \sqrt{\frac{\sum (a_i - b_i)^2}{n}} \qquad (18)$$

where a_i is the theoretical data at different frequency points, b_i is the experimental data at different frequency points, and n is the number of frequency points.

The results of the RMS error based on different unit P matrices are displayed as a dotted line in Fig. 10. In addition, the memory cost of the FEM model was recorded and shown in Fig. 10 as a dotted–dashed line.

The time costs of the theoretical 3-D FEM models with different unit periods were also recorded, as listed in Table I. The computer used in this study contains an Intel Core i7-3930K CPU and 32-GB RAM.
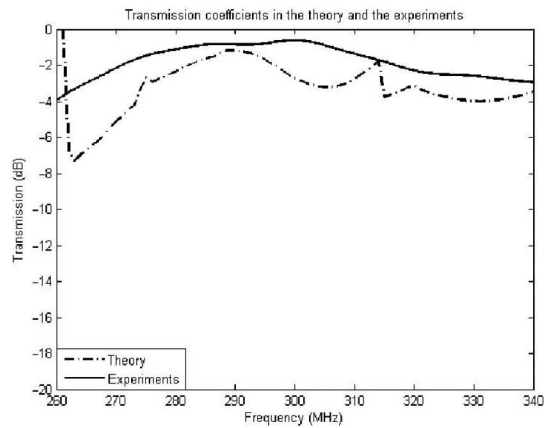
Fig. 11. Theoretical and experimental transmission coefficients.
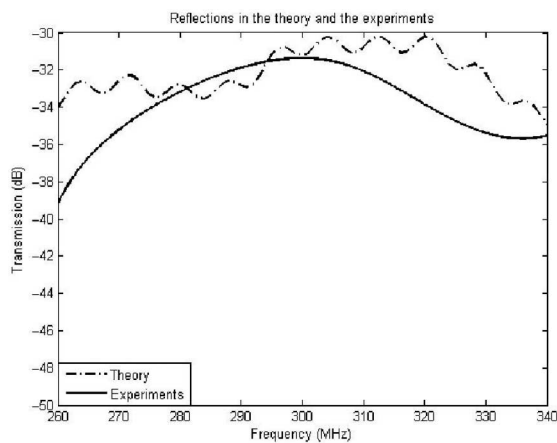
Fig. 12. Theoretical and experimental reflections.

From Fig. 10 and Table I, it can be seen that as the numbers of periods in the unit P-matrix increases to greater than 15, the variance converges. However, the time/memory cost consistently increases. Thus, considering the accuracy, time cost, and memory consumption, 25 unit P-matrix periods are large enough threshold for the P-matrix analysis.

Therefore, the transmission coefficient and reflection results based on 25 periods were adopted as the theoretical results. A comparison of the theoretical and experimental SAW transmission coefficients and reflections in the 2-D Al/128°-YX-LiNbO$_3$ PnCs is shown in Figs. 11 and 12.

Figs. 11 and 12 illustrate that the theoretical results are similar to the experimental results, which verifies the accuracy of the unit P-matrix and the effectiveness of the P-matrix analysis. Nevertheless, divergence exists outside the response bandwidth of the SAW delay lines. Fig. 9 indicates that, apart from the main lobe, the signal is weak. Moreover, it is unstable, which is strongly dependent on the time window function. Thus, the transmission and reflection of the sidelobe range may not be accurate in our experiments. Thus, we adopted the results in the main lobe from 260 to 340 MHz.

IV. Conclusion

This study introduced the unit P-matrix and its cascading to analyze SAW propagation in large 2-D piezoelectric PnCs. An example of SAW propagation was analyzed based on 150 periods of the 2-D Al/128°-YXLiNbO$_3$ PnCs using the P-matrix method, which was verified by experiments. This study compared the time/memory cost and variance of the results with different periods of PnCs in the unit P-matrix to choose the appropriate size of the unit P-matrix. The results show that based on a small unit P-matrix of 25 periods of the PnCs, the SAW propagation parameters over 150 periods can be accurately obtained using P-matrix cascading. The theoretical and experimental results exhibit good consistency, indicating the accuracy of the unit P-matrix derived by the 3-D FEM, as well as the effectiveness of the P-matrix analysis. The P-matrix analysis of SAWs in piezoelectric PnCs will promote the applications of piezoelectric PnCs in SAW devices. In the future, a 2-D P-matrix approach will be developed to obtain more accurate results which accounts for considering wave propagation in two directions.

References

[1] M. M. Sigalas and E. N. Economou, "Elastic and acoustic wave band structure," *J. Sound Vibr.*, vol. 158, no. 2, pp. 377–382, 1992.

[2] R. H. Olsson, I. F. El-Kady, M. F. Su, M. R. Tuck, and J. G. Fleming, "Microfabricated VHF acoustic crystals and waveguides," *Sens. Actuators A, Phys.*, vol. 145, pp. 87–93, 2008.

[3] I. F. El-Kady, R. H. Olsson, and J. G. Fleming, "Phononic band-gap crystals for RF communications," *Appl. Phys. Lett.*, vol. 92, no. 23, pp. 233504–233504, 2008.

[4] R. H. Olsson *et al.*, "Micro and nano fabricated phononic crystals: Technology and applications," in *Proc. IEEE Int. Ultrason. Symp. (IUS)*, 2011, pp. 983–988.

[5] Y. Y. Chen *et al.*, "Acoustic interference suppression of QCM sensor arrays utilizing phononic crystals," in *Proc. IEEE Int. Ultrason. Symp. (IUS)*, 2011, pp. 1–4.

[6] F. C. Hsu, J. C. Hsu, T. C. Huang, C. H. Wang, and P. Chang, "Reducing support loss in micromechanical ring resonators using phononic band-gap structures," *J. Phys. D, Appl. Phys.*, vol. 44, p. 375101, 2011.

[7] A. C. Hladky-Hennion *et al.*, "Design of band-stop filters using PZT layer on silicon substrate phononic crystals," in *Proc. IEEE Int. Ultrason. Symp. (IUS)*, 2007, pp. 620–623.

[8] J. H. Sun and T. T. Wu, "Guided surface acoustic waves in phononic crystal waveguides," in *Proc. IEEE Ultrason. Symp.*, 2006, pp. 673–676.

[9] J. Yoon, M. Mayer, T. Ebner, K. Wagner, and A. Wixforth, "Advanced 2D periodic array and full transversal mode suppression," in *Proc. IEEE Joint UFFC, EFTF PFM Symp.*, 2013, pp. 733–736.

[10] Y. H. Tian, H. L. Li, W. J. Tian, Y. B. Ke, J. L. Chen, and S. T. He, "A weighted waveguide for surface acoustic waves based on two-dimensional piezoelectric phononic crystals," in *Proc. IEEE Symp. Piezoelectr. Acoust. Waves Device Appl. (SPAWDA)*, 2014, pp. 375–378.

[11] M. Solal, J. Gratier, and T. Kook, "A SAW resonator with two-dimensional reflectors," *IEEE Trans. Ultrason., Ferroelectr., Freq. Control*, vol. 57, no. 1, pp. 30–35, Jan. 2010.

[12] D. Yudistira *et al.*, "Monolithic phononic crystals with a surface acoustic band gap from surface phonon-polariton coupling," *Phys. Rev. Lett.*, vol. 113, no. 215503, pp. 215503-1–215503-5, 2014.

[13] Y. Y. Zhao, H. L. Li, W. Luo, J. B. Wei, Y. Liang, and S. T. He, "Finite difference time domain analysis of two-dimensional piezoelectric phononic crystals," in *Proc. Symp. Piezoelectr. Acoust. Waves Device Appl.*, 2012, pp. 1–4.

[14] J. Q. Li, F. M. Li, Y. S. Wang, and K. Kishimoto, "Wave propagation in two-dimensional disordered piezoelectric phononic crystals," *Acta Mech. Solid Sonica*, vol. 21, no. 6, pp. 507–516, 2008.

[15] T. T. Wu and J. H. Sun, "Band gap materials and micro-phononic devices," in *Proc. Freq. Control Symp.*, 2010, pp. 515–520.

[16] V. Laude, M. Wilm, S. Benchabane, and A. Khelif, "Full band gaps for surface acoustic waves in piezoelectric phononic crystals," in *Proc. IEEE Ultrason. Symp.*, 2004, pp. 1046–1049.

[17] T. T. Wu, L. C. Wu, and Z. G. Huang, "Frequency band-gap measurement of two-dimensional air/silicon phononic crystals using layered slanted finger interdigital transducers," *J. Appl. Phys.*, vol. 97, p. 094916, 2005.

[18] T. T. Wu, Z. C. Hsu, and Z. G. Huang, "Band gaps and the electromechanical coupling coefficient of a surface acoustic wave in a two-dimensional piezoelectric phononic crystal," *Phys. Rev. B*, vol. 71, no. 6, p. 064303, 2005.

[19] H. L. Li, Y. H. Tian, Y. B. Ke, S. T. He, and W. Luo, "Analysis of Rayleigh surface acoustic waves propagation on piezoelectric phononic crystal with 3-D finite element model," in *Proc. IEEE Int. Ultrason. Symp. (IUS)*, 2014, pp. 2533–2536.

[20] Y. H. Tian, H. L. Li, Y. B. Ke, S. T. He, and W. Luo, "Extractions of reflection and velocity parameters for surface acoustic wave in two-dimensional piezoelectric phononic crystals," in *Proc. IEEE Int. Ultrason. Symp. (IUS)*, 2014, pp. 2525–2528.

[21] S. Yankin, A. Talbi, Y. Du, J. C. Gerbedoen, V. Preobrazhensky, and P. Pernod, "Finite element analysis and experimental study of surface acoustic wave propagation through two-dimensional pillar-based surface phononic crystal," *J. Appl. Phys.*, vol. 115, no. 244508, pp. 1–7, 2014.

[22] A. Khelif, Y. Achaoui, S. Benchabane, V. Laude, and B. Aoubiza, "Locally resonant surface acoustic wave band gaps in a two-dimensional phononic crystal of pillars on a surface," *Phys. Rev. B*, vol. 81, no. 214303, pp. 1–7, 2010.

[23] J. O. Vasseur, A. C. Hladky-Hennion, B. Djafari-Rouhani, F. Duval, B. Dubus, and Y. Pennec, "Waveguiding in two-dimensional piezoelectric phononic crystal plates," *J. Appl. Phys.*, vol. 101, no. 114904, pp. 1–6, 2007.

[24] P. Ventura, J. M. Hode, J. Deshois, and M. Solal, "Combined FEM and green's function analysis of periodic SAW structure, application to the calculation of reflection and scattering parameters," *IEEE Trans. Ultrason., Ferroelectr., Freq. Control*, vol. 48, no. 5, pp. 1259–1274, Sep. 2001.

[25] G. Tobolka, "Mixed matrix representation of SAW transducers," *IEEE Trans. Sonics Ultrason.*, vol. SU-26, no. 6, pp. 426–427, Nov. 1979.

[26] T. Allen, *Computational Electrodynamics: The Finite Difference Time Domain Method*, 2nd ed. Norwood, MA, USA: Artech House, 2000, pp. 285–625.

[27] R. T. Smith and F. S. Welsh, "Temperature dependence of the elastic, piezoelectric, and dielectric constants of Lithium Tantalate and Lithium Niobate," *J. Appl. Phys.*, vol. 42, no. 6, pp. 2219–2230, 1971.

Yahui Tian was born in Shandong Province, China, in 1990. She received the B.S. degree in communication engineering from Shandong University, Weihai, China, in 2012. Currently, she is working toward the Ph.D. degree at the Institute of Acoustics, Chinese Academy of Sciences, Beijing, China.

She has authored eight academic papers. Her research interests include phononic crystals and SAW devices.

Honglang Li was born in Hubei Province, China, in 1976. He received the B.S. degree in microelectronics from Hunan University, Changsha, China, in 1998, and the Ph.D. degree in acoustics from the Institute of Acoustics, Chinese Academy of Sciences, Beijing, China, in 2003.

From 2003 to 2005, he was a Postdoctoral Fellow with the Venture Business Laboratory, Chiba University, Chiba, Japan. He was an Associate Professor from 2005 to 2011 and has been a Professor since 2012, with the Institute of Acoustics, Chinese Academy of Sciences. He has authored more than 60 academic papers and applied for 25 Chinese patents. His relative application research is extended to the SAW sensors of physical/chemical/biological parameters and their applications in wireless conditions. His research interests include fast FEM/BEM analysis of the SAW sensor, optimization of SAW devices, and SAW in two-dimensional phononics crystals analysis.

Dr. Li is the recipient of a Beijing Municipal Science and Technology Award (Second Prize).

Yabing Ke was born in Hubei Province, China, in 1984. He received the B.S. degree in microelectronics and nanoelectronics from the Department of Microelectronics and Nanoelectronics, Tsinghua University, Beijing, China, in 2007, and the Ph.D. degree in acoustics from the Institute of Acoustics, Chinese Academy of Sciences, Beijing, China, in 2012.

Since 2012, he has been an Associate Researcher with the Institute of Acoustics, Chinese Academy of Sciences. He has authored more than 20 academic papers and applied for 4 Chinese patents. His research interests include fast FEM/BEM analysis of SAW devices and optimization of SAW devices.

Ce Yuan was born in Hebei Province, China, in 1991. He received the B.S. degree in applied physics from Hebei University of Science and Technology, Shijiazhuang, China, in 2013. He is currently pursuing the Graduate degree from the Beijing University of Technology, Beijing, China.

His research interests include phononic crystals.

Shitang He was born in Hunan province, China, in 1958. He received the B.S. degree in physics from Hunan University, Changsha, China, in 1982, and the M.S. degree in acoustics from the Institute of Acoustics, Chinese Academy of Sciences, Beijing, China, in 1988.

Since 1988, he has been with the Institute of Acoustics, Chinese Academy of Sciences and engaged all through in the research on surface acoustic waves (SAW) technology, including the reflection characteristics of SAW, SAW filter and filter bank, and SAW sensors. He was an Associate Professor from 1993 to 1996 and has been a Professor since 1996 with the Institute of Acoustics, Chinese Academy of Sciences. He has authored more than 100 papers and applied for 50 Chinese patents. His research interests include SAW sensors and SAW gas chromatograph.

Prof. He has received the Natural Science Award of China (Third Prize), the Natural Science Award of the Chinese Academy of Sciences (Second Prize), the Invention Award of the Chinese Academy of Sciences (Third Prize), and the Beijing Municipal Science and Technology Award(s).